

Detecting range expansions from genetic data

Benjamin M Peter^{1,*}, Montgomery Slatkin¹,

1 Department of Integrative Biology, University of California, Berkeley, Berkeley,

California 94720-3140, USA

*** E-mail: bp@berkeley.edu**

Abstract

We propose a method that uses genetic data to test for the occurrence of a recent range expansion and to infer the location of the origin of the expansion. We introduce a statistic for pairs of populations ψ (the directionality index) that detects asymmetries in the two-dimensional allele frequency spectrum caused by the series of founder events that happen during an expansion. Such asymmetry arises because low frequency alleles tend to be lost during founder events, thus creating clines in the frequencies of surviving low-frequency alleles. Using simulations, we further show that ψ is more powerful for detecting range expansions than both F_{ST} and clines in heterozygosity. We illustrate the utility of ψ by applying it to a data set from modern humans and show how we can include more complicated scenarios such as multiple expansion origins or barriers to migration in the model.

Author Summary

Many important biogeographic processes can be interpreted as range expansions, where a species is constraint to a small local habitat in the beginning and expands from there to colonize a larger region. Examples of this include biological invasions, the spread of infectious diseases and humans colonizing the world. We present a statistical framework to test for the existence of such an expansion and examine its properties. We then use this framework to make further inference, and show how it can be used to estimate the origins of the range expansion and to identify barriers of gene flow.

Introduction

Range expansions are ubiquitous in natural populations, and they are responsible for numerous biological phenomena. Range expansions result in a series of founder events that cause the newly founded

populations to differ genetically from the source population. Some well-known examples are biological invasions [1], the post-ice age patterns of migration in several European [2, 3], and the colonization of Eurasia and North and South America by modern humans [4–6]. In some cases descendants from the source population remain near the location of the ancestral population. For example, the European population of the brown bear *Ursus arctos* most likely survived the last ice age in refugia in Spain and Greece. Brown bears followed the receding glaciers to colonize most of Europe, but populations at the locations of the former refugia persisted until the populations were driven to the verge of extinction by humans in the 20th century [7]. Another example are humans, where derived populations are found all over the world, but there are also descendants of the first humans still living in Africa.

Sometimes, the routes of migration are known from direct observations, historical records and archaeological evidence. Frequently, however, the exact history of a species is unknown, and we want to use population genetic methods to gain more information. In this paper, we use genetic data to address two related problems: detecting whether a range expansion has occurred and inferring the geographic origin of a range expansion.

Characterizing the influence of geographic structure on genetic diversity has been one of the major goals of population genetics theory, with important contributions from Wright [8], Malécot [9], Kimura [10] and many others. While there are many statistics designed to infer differentiation between populations [11–14], the most widely used statistic to detect differentiation between populations is the fixation index F_{ST} , which traces to Wright [15]. A variety of estimators of F_{ST} have been developed (e.g [13, 16]). Roughly speaking, F_{ST} measures how much diversity exists between subpopulations compared to the diversity in the entire population; a value of 0 indicates that the two subpopulations are indistinguishable, whereas a value of 1 indicates that two populations are maximally differentiated. F_{ST} has been directly linked to the migration rate in several models, including the finite island [17] and stepping-stone models [18]. Although F_{ST} can be used to quite accurately estimate the amount of gene flow between equilibrium populations, it cannot be used to infer directionality of gene flow.

Two other methods that are widely used to detect geographic patterns are clustering algorithms and ordination methods. Clustering analyses [19–22] such as STRUCTURE [19]) classify individuals into discrete groups, which can then be used for further analysis. Ordination techniques [23], such as principal components analysis and multidimensional scaling summarize data by indicating the overall similarity of populations. Principal component analysis has been shown that genetic diversity relatively closely

56 correlates to the geographic distribution of humans on a continental [24] and global [25,26] scale.

57 It is also possible to use likelihood methods to infer past features of population history. For example,
 58 the program IM [27] estimates the time of separation of populations and migration rates between them
 59 using data from multiple unlinked loci, and the program *dadi* [28] estimates past rates of population
 60 growth from the joint allele frequency spectrum from two or three populations. Both of these programs
 61 are computationally intensive and neither can analyze data from numerous populations.

62 Most statistics applied to subdivided populations do not provide information about asymmetries.
 63 F_{ST} and most genetic distances are defined in such a way that they are commutative (i.e. F_{ST} between
 64 populations A and B is the same as F_{ST} between B and A), and hence the value depends only on the
 65 amount of migration, not whether migrants moved mostly from A to B or from B to A. Clustering
 66 algorithms can produce groupings of populations that can be interpreted as describing an expansion, but
 67 the expansion-specific information is lost in the process and the results of clustering is often sensitive
 68 to tuning parameters such as the number of clusters. For principal components analysis, the view that
 69 the first principal component axis follows the direction of expansion [29] has recently been challenged
 70 [22, 24, 30], and it has recently been shown that, depending on parameters and the locations of the
 71 populations sampled, the first principal component axis might be parallel to or orthogonal to the axis of
 72 expansion, or at an angle in between.

73 Population genetics theory has shown that a range expansion can be detected from the characteristic
 74 reduction in genetic diversity with increasing distance from the origin of the expansion [5, 31–35]. The
 75 reason is that the succession of founder events during the expansion cause the progressive loss of genetic
 76 variants. This prediction has been confirmed by comparing the numbers of mtDNA haplotypes found in
 77 Southern European refugia and in central Europe [7]. The same pattern can also be seen in humans
 78 where both a reduction in heterozygosity and an increase in linkage disequilibrium with increasing distance
 79 from the presumed origin of the expansion in Africa can be shown [5].

80 In addition to creating a gradient in genetic diversity, range expansions tend to create clines in the
 81 frequencies of neutral alleles, with the frequency increasing on average in the direction of the expansion
 82 [35]. An intuitive reason for this pattern is that each founder event results in additional genetic drift,
 83 and populations further away from the origin of expansion will therefore have experienced more genetic
 84 drift. This can be seen from the following simple argument: The expected frequency of an neutral allele
 85 in the new population is the same as in the source population. But some alleles will have zero frequency

in the new population. Therefore, the average frequency of shared alleles, i.e. alleles that are present in the new population, is expected to be higher than in the source population, thus creating the cline. This observation provides the foundation for our method of detecting range expansions.

In this paper, we introduce a statistic, the directionality index ψ , for pairs of populations. ψ is sensitive to patterns created by range expansions as it detects clinal patterns created by successive range expansions. We show, using simulations, that the expectation of ψ is zero in an equilibrium isolation-by-distance model, and that positive values of ψ indicate the direction of the expansion. We also show that if we have multiple samples, ψ can be used to infer the origin of a range expansion and the location of barriers of gene flow. We also explore the power and robustness of our methods and finally apply it to human genetic data.

Results

In this section, we will define the directionality index, give an intuitive explanation and discuss some of its properties. We will show that the directionality index is sensitive to recent range expansions in a one or two dimensional stepping-stone model, and then explore some more advanced applications.

Definition Of The Directionality Index

Consider two samples of size $n, n \geq 2$ taken from two subpopulations S_1, S_2 . Each sample consists of L biallelic markers (e.g. SNPs) that are shared between S_1 and S_2 . The directionality index is defined as

$$\psi = \frac{1}{n} (\bar{f}_{S_1} - \bar{f}_{S_2}) = \frac{1}{Ln} \sum_{l=1}^L (f_{S_1,l} - f_{S_2,l}), \quad (1)$$

where \bar{f}_S is the average allele frequency of all alleles in population S , and $f_{S,l}$ is the number of derived copies of allele l in the sample from population S . Equivalently, ψ can also be defined in terms of the two-dimensional site frequency spectrum (2D-SFS):

$$\psi = \sum_{i=1}^n \sum_{j=1}^n (i - j) f_{ij}. \quad (2)$$

where f_{ij} denotes the proportion of SNP in the sample that are at frequency i in S_1 and at frequency j in S_2 , and the SFS is normalized such that $\sum_{i < j} f_{ij} = 1$.

$$\psi = f_{21} - f_{12}. \quad (3)$$

The three different definitions represent different interpretations of the directionality index, and it is useful in building an intuition to discuss them briefly: Equation 1 corresponds to the definition alluded to in the introduction, where we compare the average allele frequency between the two populations. As the population further away from the expansion origin is expected to have experienced more genetic drift, its alleles are expected to be at a higher frequency and thus ψ is positive if $\bar{f}_{S_1} > \bar{f}_{S_2}$ and S_1 is further away from the origin of the expansion. If both populations have experienced similar amounts of genetic drift, then the allele frequencies will be equal, $\psi \approx 0$ and we will not detect an expansion. Equation 2 is based on the SFS, and we see that ψ will be positive if f_{ij} is usually greater than f_{ji} . Thus, we are comparing the SFS entries that are mirrored along the $x = y$ diagonal, and the directionality index measures the “skew” in the 2D-SFS. If there are more SNP that fall in the upper left triangle of the SFS (where $j > i$), ψ will be negative, and we infer an expansion from S_1 to S_2 . The inverse conclusion will be drawn if there is an excess of SNP in the lower right triangle, and if the SNP are distributed symmetrically around the $x = y$ diagonal, ψ will be zero. Much of the paper will be focused on the case where each population is represented by a single genome, a case we think will be particularly common in many analyses. In this case, equation 2 reduces to 3 and we are simply comparing the abundance of SNP that are fixed for the derived allele in sample S_1 and heterozygous in S_2 to the number of SNP that are heterozygous in S_1 and fixed in S_2 . If either number is significantly larger than the other, we infer migration in the direction of the larger number. It is also worth noting that the computation cost of equation 1 scales proportionally to the number of loci in the sample, whereas equation 2 only depends on the sample size squared. Thus, for genome scale data sets where $L \gg n^2$, (2) will be much faster to compute.

Determining Whether A Range Expansion Occurred

We first test the power of ψ to distinguish pairs of populations sampled from a recent range expansion to pairs of populations sampled under isolation-by-distance at equilibrium in a 1D-model. Figure 1

shows that F_{ST} increases at approximately the same rate under an equilibrium stepping-stone model with only isolation-by-distance (Panel A) and a model with a range expansion (Panel B), indicating that the two scenarios are comparable. We see that ψ is constant at zero in the isolation-by-distance model, regardless of the distance between the samples. In contrast, ψ increases with distance under the expansion model, due to the increase in allele frequency along the expansion axis. Interestingly, ψ increases almost linearly with the distances between the origin and the population sampled, a fact we exploit in the next section to infer the origin of the expansion. We also plotted the heterozygosity, a statistic that is also expected to be constant under an equilibrium model [36] and increasing under an expansion [5, 31]. However, our simulations show that heterozygosity is larger in the center of the habitat than near the boundaries because of the boundary effects. This is in contrast to most theoretical results [36] which either assume either a circular model or an infinitely long stepping stone model, and where the heterozygosity is independent of the sampled deme. However, the observed gradient in heterozygosity has been observed previously and explained by longer coalescence times for a sample taken close to the boundary [37, 38] and it is worth noting that this effect is much weaker in a two dimensional population.

On the other hand, F_{ST} and ψ behave in similar ways in both 1D and 2D models (Figure 2). F_{ST} is slightly larger in the case of a range expansion than in the isolation-by-distance model (Panels A and C), but qualitatively we see an increase of F_{ST} with distance under either model. The pattern for ψ , however, is again different (Panels B and D): under the isolation-by-distance model, ψ is smaller than 0.01 for almost all comparison, with the exception of a few demes that are at the boundary of the simulated region. In contrast, the magnitude and sign of ψ nicely illustrate the effect of the range expansion. ψ is zero only for demes that are very close to each other or demes that are equally far away from the expansion origin. The latter can be explained by symmetry: two samples that are an equal distance apart from the origin will have a symmetric SFS, resulting in a ψ close to zero.

Various significance tests can be used to determine the significance of ψ between two populations; for the case of $n = 2$ in both samples we can simply perform a binomial test on the absolute frequencies f_{21} and f_{12} . If their proportions differ significantly from 0.5, we can reject the null hypothesis of symmetric migration between the two demes. When comparing samples of size $n > 2$, we can generate a null distribution using a permutation test, i.e randomly assigning the allele frequencies for each SNP to either population. However, both these tests will underestimate the variance in the data if SNPs are not in linkage equilibrium. In that case the “effective” number of loci will be lower than the actual number. To

162 take linkage into account we use a computationally more intensive block-jackknife approach [39, 40] to
 163 analyse our real data.

164 In Figure 3 we show the effect of the most important parameters on our ability to reject the null
 165 hypothesis of isolation-by-distance for pairs of samples of size two. For all parameters, we find that using
 166 the directionality index results in higher power than comparing differences in heterozygosity, while false-
 167 positive rates are low and roughly the same for the two methods. We find that we have comparatively
 168 little power to reject the null hypothesis if the two sampled individuals are close to each other (Panel
 169 3A). This is expected, since there are fewer founder events separating the two individuals. Therefore
 170 we expect ψ to be lower for nearby populations, as shown in Figures 1 and 2. Panel B shows that
 171 a moderate number of shared SNPs is necessary, i.e. more than one thousand, to get high power to
 172 reject equilibrium isolation-by-distance. In addition, we find that slow expansions are harder to detect
 173 than rapid expansions, and more recent expansions are easier to detect than expansions that happened
 174 a long time in the past (Panels C and D). Neither of these findings is unexpected; after an expansion
 175 genetic drift will affect the loci in both populations equally. The number of shared SNP that are due
 176 to the range expansion will decrease with time and be partially replace by SNP that only experienced
 177 the equilibrium model and hence do not carry a signal of the expansion. Similarly, if the time between
 178 expansion events is high, the founder effects caused by the expansion will become less important relative
 179 to genetic drift between expansion events, weakening the signal of the expansion. In this scenario, the
 180 power of heterozygosity to detect an expansion decays much faster than the power of ψ . Finally, we note
 181 that the false positive rate, denoted in grey and pink in Figure 3, is independent of both the distance
 182 between loci and the number of SNPs.

183 Inferring The Origin Of A Range Expansion

184 In addition to showing that range expansion occurred, the results in Figures 1 and 2 suggest that spatial
 185 patterns in pairwise values of ψ can indicate the origin of an expansion if we have more than two
 186 samples. For this purpose, we employ a method commonly used by engineers in problems of localization
 187 and navigation [41], called Time Difference of Arrival location estimation (TDOA). TDOA methods are
 188 used in remote sensing and to locate cell phones [41]. The key assumption of the TDOA algorithm is
 189 that the magnitude of a pairwise statistic between two sample locations i and j is proportional to the
 190 difference in distance from i to the origin and the distance from j to the origin. So, if i is very close

191 to the origin and j far away, then we would expect the TDOA statistic to be large, but if i and j are
 192 at the roughly the same distance from the origin, then the TDOA statistic should be close to zero. In
 193 engineering applications the TDOA statistic is the time difference between the arrival of a signal emitted
 194 from the origin (hence the name). In our application, however, ψ takes on the role of the time difference
 195 with the implicit assumption that the directionality index between locations i and j , ψ_{ij} , is proportional
 196 to the difference in distances from i and j to the origin, respectively. To further illustrate how we can
 197 use this method to infer an origin, we first consider the special case of $\psi_{ij} = 0$. Assuming that we have
 198 already rejected isolation-by-distance, we know that i and j are equally far from the origin and the origin
 199 must therefore lie on the line perpendicular to the line through i and j .

200 If we had three or more loci all at the same distance from the origin (so that the pairwise ψ values
 201 are all zero), we could thus infer the origin as the center of the circle passing through the three points.
 202 In general, however, ψ will be non-zero. In that case, we know from elementary geometry that the set of
 203 candidate points based on a one pair of samples is not a straight line, but a hyperbola with i and j as its
 204 focal points. If we have samples from k locations, we can calculate ψ for $k(k-1)/2$ samples and hence
 205 obtain $k * (k-1)/2$ hyperbolas. In a perfect, noiseless world, all hyperbolas would intersect in a single
 206 point: the origin of the expansion, as illustrated in Figure 4. In practice, of course, genetic data is highly
 207 stochastic and we have to estimate the origin. To do this, we interpret each hyperbola as a non-linear
 208 equation with three unknowns, the sample coordinates x, y and the speed of expansion v . v is a nuisance
 209 parameter that describes how much the allele frequency increases per unit distance from the origin. For
 210 more than three samples the system is overdetermined and, rather than solving the system of equations
 211 explicitly, we use weighted non-linear least squares.

212 We first illustrate this approach on simulated data, where we sample a regular grid (Figure 5. We
 213 simulated a range expansion in a 101 x 101 stepping stone model. In all simulations, we chose the
 214 coordinate system such that each deme corresponds to one unit of distance. The start of the expansion
 215 is in deme (25,35), indicated by the grey dotted lines in Figure 5. The direction of the arrows plotted in
 216 Figure 5 indicate the sign of the pairwise ψ -value, between adjacent samples on a grid, and the thickness
 217 of each arrow corresponds to the magnitude of ψ . A missing arrow denotes a non-significant ψ value.
 218 In Panel 5A we performed a simulation under an equilibrium isolation-by-distance model. We see that
 219 in this scenario, only 11 out of the 60 pairwise comparisons are significant; all of them point towards
 220 the corners and are due to the boundary effects of the simulations. The red ellipse is a 95% confidence

221 ellipse of the inferred origin. Under the isolation-by-distance model, this is located in the center of the
 222 population, illustrating that the TDOA approach will yield an answer even if there is no expansion has
 223 occurred, so it is important to first test if an expansion has actually occurred. From Panels B-D we see
 224 that the expansion signal is clearly portrayed by the directionality indices and we get high confidence in
 225 the estimated origin. In fact, the confidence is so high that the ellipse is barely visible in Panel B, but
 226 confidence decreases when we reduce the number of samples. Furthermore, we see from Panels C and D
 227 that the origin is slightly biased towards the center of the population. This is again due to a boundary
 228 effect, and goes away if we take all samples at least 10 demes away from the boundary of the population.

229 To assess the properties of this method more systematically, we report root mean squared error
 230 (RMSE) under several scenarios (Figure 6). We also compare our method to the method of Ramachandran
 231 et al. [5], who used linear regression of the heterozygosity on the distance to candidate origins. Their
 232 inferred origin of the expansion is the point with the highest associated regression coefficient, conditional
 233 on the slope of the regression curve being negative. Most data in Figure 6 was simulated with a fairly
 234 rapid expansion; the time between subsequent expansion events was set to 0.001 coalescence units, so
 235 that the complete expansion was completed in 0.13 coalescence units. This speed is roughly equal to the
 236 out-of-Africa expansion of humans. For these parameters (Figure 6A-D) the two methods have similar
 237 performance, with only marginal improvements in how the methods perform with different amounts of
 238 data. We find that with adequate numbers of samples and data, the RMSE for both methods is around
 239 four, with less than one distance unit of difference between the two methods. Overall, the ideal amount of
 240 data for this method lies around 20 diploid samples and 7,000 independent SNPs. Increasing the amount
 241 of data beyond this level will not substantially improve performance. For the set of simulations with
 242 increasing numbers of SNPs, we also tested the effects of sampling on a grid versus taking samples from
 243 random locations. It might be assumed that the latter scenario is closer to a realistic sampling scheme.
 244 Interestingly, we found only negligible differences, indicating that the sampling locations are only a minor
 245 issue unless the sampling locations are very skewed (e.g. a transect sample).

246 Changing the position of the origin has little effect on the RMSE for the first 30 distance units,
 247 indicating that we have good accuracy if the origin is not close to the border. If there is an expansion
 248 that started outside the sampled range, the method will perform significantly worse. This has two causes:
 249 first, we would expect it to be easier to infer the origin if it lies in the middle of the sample, as compared
 250 to an origin that is far away from all samples. This part also explains the difference between samples

taken on a grid and random samples: In the grid, the corners are systematically sampled (since we force a grid sample to be there), whereas in many random samples there may be fewer samples on one side of the origin than on the other, resulting in a loss of accuracy. A second factor resulting in reduced accuracy are again boundary effects, which skew the effect of the expansion if it happened close to the boundary.

We focus our attention on the effect of the parameters of the expansion (6C-F): The number of founders (Figure 6d) has an almost linear effect on the estimation accuracy. Fewer founders imply a stronger founder effect and hence a stronger signal of expansion [35], which makes the origin easier to detect. We find the biggest difference in how our method performs in comparison to the Ramachandran method when slowing down the expansion, or when we want to detect an expansion that occurred some time in the past. Interestingly, our method performs at almost the same accuracy independent of the expansion speed, whereas the accuracy of the Ramachandran method declines faster. Also, we find that the heterozygosities approach equilibrium soon after the expansion has finished (6F), whereas the shared alleles used by ψ keep the signature of the range expansion for much longer.

Adding Environmental Complexity

The previous section assumes an idealized population in a homogeneous habitat. In practice, however, habitats are heterogeneous and barriers to gene flow and pathways of expansion are often very important. In the following sections, we show how our method performs in slightly more complex scenarios. First, we allow demes with different population sizes. While we kept the mean size of demes the same, we followed [42] in drawing deme sizes from a gamma distribution. A second important feature not present in the previous simulations are barriers to dispersal that affect both the initial expansion and gene flow following the expansion. Depending on the species, these barriers may correspond to rivers, mountains or even roads. We illustrate how we can use graph algorithms and the directionality index to identify them. Finally, we explore the case with an expansion starting from multiple points, and how we can infer the coordinates of the origins.

Heterogeneous Population Sizes

The effect of variance in deme size on demographic expansions was explored extensively in a simulation study by Wegmann et al. [42]. They found that heterogeneous populations have a higher rate of population differentiation between demes, and predicted that detecting range expansion would be more difficult

because of the increased noise. Our simulations confirmed this prediction but only if there is substantial variation in deme size. We found that heterogeneity in deme size has little effect if the variance in deme size is low, with RMSE only differing slightly from the case with equal deme sizes. A variance of 0.5 in deme size, for example, corresponds to a size difference of around two orders of magnitude between the largest and smallest deme. But the average RMSE for the location estimate only increased to 5.43, compared to 4.57 in a comparable scenario without variation in deme size. However, this value corresponds to some kind of “tipping point”: when we further increasing the variance in deme size, some deme sizes will become effectively zero in size and this greatly reduces the accuracy of the location estimate, indicating that significant barriers to gene flow make our location estimate less precise.

Barriers

We can use pairwise directionality indices to gain information about colonization paths, i.e. the corridors through which the population expanded. We approach this problem by interpreting a set of pairwise directionality indices as a directed graph, where the samples correspond to the vertices and the directionality indices correspond to the edges connecting the samples. To achieve a visual representation of the graph, we apply graph algorithms to remove some of the edges. In particular, we use the transitive reduction algorithm [43]. A transitive reduction finds the graph with the fewest edges that retains the connectivity of the original graph. That is, if there is an edge from vertex v_1 to vertex v_2 , but there is also an indirect path from v_1 to v_2 via another vertex v_3 (i.e. ψ is significantly negative between v_1 and v_3 as well as between v_3 and v_2), then the edge from v_1 to v_2 is removed from the graph. A further reduction can be obtained by computing a maximum spanning tree [44], which reduces the graph to $n - 1$ edges, where n is the number of samples. The maximum spanning tree representation should be able to identify major migration paths, and does not cross strong barriers of gene flow (Figure 7). Furthermore, we can obtain an ordering of all samples by simply summing all ψ values that sample is involved in:

$$\psi_i = \sum_{j \in \text{samples}} \psi_{ij}. \quad (4)$$

The lowest value of ψ_i among the samples denotes the sample that was taken closest to the origin, and the highest value of ψ_i is the sample furthest along the expansion. In Figure 7B we show that both the maximum spanning tree and the ordering are useful tools and able to identify the barriers.

Multiple Origins

Range expansions may have more than one source. A classical example is the colonization of Central Europe after the last glacial maximum. Species with Southern European refugia in the Balkan Peninsula, Italy or the Iberian peninsula followed the receding glaciers and explain many biogeographical patterns we observe today [3]. Our method extends in a straightforward manner to such expansions. The key idea is to first find samples that were predominantly colonized from a single origin, and then estimate the position of that origin independently. There are several ways to assign sampled individuals to clusters corresponding to a single origin. In classical studies, often mtDNA haplotypes were used for this purpose (e.g. [2,7]), but programs such as STRUCTURE [19] or simple clustering based on the observed polymorphism frequencies may yield more accurate results. In our simulations, a simple K-means clustering algorithm was able to correctly identify the number of clusters in all cases, even when the two founder populations were drawn from the same original population. The resulting estimates of the origins are slightly less precise than with a single origin (Figure 8), but that is to be expected as there are fewer samples contributing to the location estimate for each origin. Also, the estimates were worse when the two origins were close together.

Application

Human Diversity

We applied our method to a data set from 55 human populations from the Human Genome Diversity Panel and HapMap III [45–47]. We calculated ψ and its standard error for all pairs of populations and transformed this into a Z-score. As expected from a data set with several hundred thousand loci, the vast majority of comparisons were highly significant, with a median absolute Z-score of 28.1, and a mean absolute Z-score of 41.9 across all comparisons made. Globally, we could make out four major clusters of populations: i) Africans, ii) Europeans and Pakistani, iii) East Asians and iv) Native Americans. Overall, every one of the 450 comparisons made between a population in Africa and Non-African showed evidence for gene flow out of Africa, confirming the out-of-Africa hypothesis. Within Africa, we found all comparisons to be significant, and all pairwise ψ values agreeing on a single origin of the expansion. The San people were the only population that had positive ψ values when compared to all other populations, indicating that they are closest to the origin of humans. They are followed by the Biaka- and Mbuti-

pygmies, which have negative ψ values when compared to the San. This is followed by the southern Bantu sample, and a cluster consisting of Yerubans, Luhya, Mandenka and Northern Bantu, each having a negative ψ for other previously mentioned populations, and positive scores for all other populations. The African populations furthest away from the origin were the Maasai and Mosabite, the latter being very distinct from the sub-Saharan populations.

The closest populations outside Africa are the Bedouin and Palestinian populations, both from the Middle East. The third Middle Eastern population present in our data, however, the Druze people, fall in a large cluster containing almost all European, Pakistani and Indian populations. Within Europe, the three Italian population samples all have non-significant ψ scores, but are found to be more ancestral to the other European populations. They are followed by the French and French-Basque, which also cannot be distinguished, and the Orcadian, Adygei and Russians. In Pakistan, we find the Makrani to be the most ancestral population, followed by the Brahui and Balochi, Sindhi, Kalash and Burusho. It is noteworthy that this list corresponds to their distances from Africa, with the exceptions that the Brahui and Balochi are switched, and the Hazara are not in the main Pakistani cluster, but rather form a distinct group with the Uygur. Besides the Uygur, all other East Asian populations form a single large cluster with very little resolution. Clearly distinct from this cluster are the Papuans and Melanesians, which are very similar with asymmetry between these two populations ($\psi = 0.0019$, $SE\psi = 9.2e - 4$, $Z = -2.05$). They are closer to the Africans than to the East Asians, but further away than the Pakistani and European populations.

Finally, Native American populations form a distinct cluster, which are strongly separated from all other populations. Within the Native American populations, we find evidence of a North to South colonization pattern with Pima being closest to the Eurasian populations, followed by the Maya and Colombians. The most distant populations are the South American Karitiana and Surui, which have a nonsignificant pairwise ψ between them.

We also tested our ability to infer the origin of humans using the TDOA approach. As continents most likely act as strong migration barriers, we did not use the TDOA approach on the entire HGDP data set. Instead, we applied our method to the data set of Henn et al [48] which contains 30 African populations. We estimate an origin of the Human expansion at 30° S 13° E, which lies in central South Africa, closest to the San sample locations at 28.5° S 21° E and 22° S 20° E, respectively.

Discussion

In this paper, we introduced a new statistic, the directionality index ψ . We then showed that ψ can be used to reject an equilibrium isolation-by-distance model, and we used it both to characterize a range expansion and estimate its origin. Although we have focused on range expansions, ψ is sensitive to other deviations from symmetric migration. While a range expansion might be a plausible explanation in many cases, alternative scenarios such as a source-sink population structure or a large differences in effective population sizes should also be considered. One of the main advantages of the simplicity of the directionality index is that the assumptions - and limitations of the approach are easy to discern: the directionality index is zero if the 2D-SFS is roughly symmetric about the diagonal. This is certainly true under most models considered in theoretical studies, such as island and stepping stone models, particularly as the boundary conditions in the latter are typically chosen such that the model is symmetric. The directionality index can be used to determine how appropriate these models are for a given data set. If ψ differs from zero then care should be taken in applying methods that are based on these theoretical models. On the other hand, if ψ is close to zero, we can interpret this as justification for using the powerful theoretical results for these models [36].

In this regard, the directionality index can be seen as a “first step” analysis that can be computed very easily, is able to answer very broad questions about our data and then be used as a guide to which more complicated parametric models might be employed, e.g. in an Approximate Bayesian Computation [49,50] or dadi [28] framework. We have also shown how we can introduce the physical location of the samples in our inference framework. In many cases, natural populations are better described by a continuous distribution [51,52], and as we show in the TDOA analysis, using a simple statistic together with the physical locations can result in a quite powerful method. Our approach is also different from most other methods dealing with spatial data in that it explicitly assumes a non-stationary population. In this paper, we link the ancestral demographic process of a range expansion to the observed patterns of genetic diversity. While the effect of the expansion on F_{ST} appears to be quite small, our ψ statistic can be used to distinguish between equilibrium and non-equilibrium models. Finally, we also show how we can extend our method to deal with complications. Whereas the TDOA analysis is not robust to large barriers of gene flow, interpreting the pairwise ψ statistics as a graph can unmask important details of a species’ history.

Simulation Results

We find that the directionality index ψ is well suited to distinguishing between isolation-by-distance and range expansion when demes are sufficiently far apart and the range expansion is recent and occurs at a fast rate. These restrictions are not surprising. Geographically close demes will be genetically more similar, regardless of their history, and historical processes should therefore be harder to distinguish. That a recent expansion is easier to detect than an older one is also easily explained by the eventual convergence to equilibrium isolation-by-distance pattern, and similarly, a rapid range expansion leaves less time for genetic drift to blur the patterns created by the range expansion. Lastly, increasing the amount of data will increase the power to distinguish asymmetric from symmetric processes as each single SNP contributes only a little information about the history of dispersal. In all cases, our ψ statistic outperforms ΔH . From the analyses under the stepping-stone model we see one of the main differences between ψ and genetic distance measures, such as F_{ST} . In an isolation-by-distance model, F_{ST} will increase with distance, but ψ will not deviate from zero as the distance between the sampled locations increases. Again, this makes sense intuitively: The number of shared genetic variants decreases with distance, and hence F_{ST} increases. However, this reduction in shared polymorphisms is symmetric, and hence will have no effect on ψ . The pattern is different in the model of a population expansion: when comparing with a sample from the origin of expansion, both F_{ST} and ψ increase with distance. The signal diminishes, when migration rates are high, however. This is apparent from Panel D in Figure 1, where ψ is zero for the first ten demes. Here, migration had enough time to undo the effect of the range expansion in the demes that are further away from the origin.

In the origin estimation section, we find that we can get surprising accuracy with relatively little data. 20 samples with around 10,000 SNP yield accurate estimates. This amount of data indicates that our method is not applicable to mtDNA or microsatellite data, but it should be applicable to transcriptome data, which can be assembled for many non-model organisms. It is also worth noting that the error does not go to zero even with larger amounts of data. This can have several reasons. A big contribution is likely from the linearity assumption we made for the TDOA approach. ψ does not increase perfectly linearly with distance, and especially the boundaries of the simulated region may introduce a considerable bias. A second, more subtle point is the algorithm we use; whereas least-squares is very easy to use and yields good results, other optimization algorithms might reduce the RMSE. A third explanation is that genetic processes are simply very noisy, and we require much more data to obtain better results. Our

421 results also show that using heterozygosity to infer the origin of an expansion is largely similar to our
 422 statistic for recent, fast expansions.

423 We demonstrated how our method can be adapted to incorporate more complex models. We showed
 424 that small differences in deme sizes have little influence on our ability to estimate the origin. If however,
 425 the habitat is very heterogeneous our method becomes less accurate. This implies that some care must
 426 be taken when for example analysing endangered species with very patchy habitats, or species whose
 427 dispersal distance is much lower than the size of a local population, or when analyzing global patterns
 428 of diversity. If there are strong barriers to the gene flow, the TDOA method should not be applied, as
 429 its central assumption that ψ is proportional to physical distance is violated. In that case, while it is not
 430 possible to infer an origin that is distinct from the samples, it is nevertheless possible to find the sample
 431 that is closest to the origin, which in many cases might suffice to support or reject a hypothesis. Also,
 432 we have shown that we can apply graph algorithms to get a representation of the migration pattern that
 433 leads to meaningful interpretation.

434 Human Genetic Diversity

435 When analysing the human data sets, we found that i) ψ scores are correlated with distance and ii) if
 436 population i is closer to Africa than population j , then $\psi(i, j)$ is in most cases negative, a pattern that
 437 is expected under a model of expansion from Africa. As explained previously, the directionality index
 438 depends not only on the two population compared but also on the history of the other populations. We
 439 find the South African San people to be the population closest to the origin of humans both using the
 440 TDOA method and when interpreting all pairwise directionality indices. This supports the interpretation
 441 that the origin of modern humans is somewhere in Southern Africa [6, 48]. Another interesting result is
 442 that the Melanesian and Papuan samples, while very similar, show positive ψ values when compared to
 443 other East Asian populations, but the directionality index is negative when compared to the Pakistani,
 444 European and African populations. This is consistent with a “two-wave” model of colonization of South-
 445 East Asia, with a first wave consisting of present-day Papuans and Melanesians, and a second wave
 446 consisting of the present day Chinese populations [53].

Methods

Simulations

We implemented a simulator that performs continuous time coalescent simulations on a discrete stepping stone model [9, 10] of finite size. We assumed that the backward migration rates were equal between all pairs of adjacent demes and that the boundaries were reflecting. We used a modified version of the expansion model of [35], where an expansion is modeled with a one-generation bottleneck of reduced size. In our backward-in-time framework, this corresponds to moving all lineages present in a deme being colonized to a randomly chosen neighboring deme. We introduce a founder effect by adding additional coalescence events according to the appropriate backward Wright-Fisher transition probability (Page 62 in [54]). Unless noted otherwise, all expansions were done with a founder size of 200. Once the final deme is reached, an regular island model coalescent is run where each island corresponds to a founder population (in most simulation, the number of islands is one).

Throughout this paper, we simulated unlinked SNPs using an importance sampling scheme. After generating 1,000 gene trees, we calculate the appropriate multi-dimensional site frequency spectrum, where each sampled population corresponds to a dimension. We can then draw SNPs with replacement from this site frequency spectrum.

The parameters used for the majority of power simulations are as follows: We simulated on a 101 x 101 stepping stone model, with deme coordinates starting at (-50,50) at the lower left corner and (50,50) in the upper right corner. Each deme exchanges migrants to the neighboring demes to the north, south, east and west at rate $M = 1$. For the power simulation, we sampled a single diploid individual each from two colonies at (-25,-25) and (-25,25). For the TDOA simulations we simulated one individual each from a deme on a quadratic grid between (-30,-30) and (30,30), with 36 samples in total. This corresponds to a distance of 12 demes between any two sampled demes. We usually generated 1,000 independent coalescent trees and then used importance sampling to generate 100,000 SNP from the population, conditioning on them being shared between at least two of the samples. In the case of a range expansion, the standard point of origin was set to (-15,-25) and the expansion occurred at a rate of one expansion event every 0.001 coalescence units, with the expansion being observed 0.13 coalescent units after it started, where coalescent units are measured on the time scale of a local deme. These parameters were chosen to roughly correspond to the human out-of-Africa expansion. The directionality index ψ and F_{ST} were calculated

in Python; for ψ we used equation (2), and F_{ST} was estimated using Reynold's estimator [13]. Note that these are only baseline parameters, and exploring the effect of changing these parameters is the main purpose of most of our power simulations.

To generate data for the 1D stepping stone model analyzed in Figure 1, we simulated a 201×1 habitat, with scaled migration rates $M = 1, 10$ between adjacent demes. Sampling was done in demes $-i/2$ and $i/2$, with the center deme having coordinate 0. In case of range expansions, the expansion started in deme $-i/2$.

SNP ascertainment may influence our results, because most ascertainment schemes favor high frequency alleles in the populations where the ascertainment was performed. To assess the effect of ascertainment bias on the value of ψ , we performed simulations in an isolation-by-distance model with samples at coordinates (0,0), (10,0), (20,0), (30,0), (40,0), (50,0) as well as (0,10) and (15,10) and then computed ψ between the (10,0) and (20,0) sample. We then simulated ascertainment by selecting a set of population, and rejection sampling SNP so their 1D-SFS followed a Beta(2,4/3) distribution, which roughly matches the SFS in the HGDP data set and is very different from the expectation without ascertainment bias. If ψ differs significantly from zero, then we know that ascertainment is important. Results are given in Figure S1; ascertainment is important if it is performed in one of the populations that we calculate ψ for. However, the effect of ascertainment is negligible if the population we calculate ψ for are different from the ascertainment population, even if the ascertainment population is much more closely related to one population compared to the other.

Estimating the origin of a range expansion

We use a time-difference of arrival (TDOA) approach [41] to estimate the origin of a range expansion. TDOA was originally used in naval navigation during the Second World War, and is currently widely used to solve localization and navigation problems. It is based on the assumption that a single source emits a signal that decays with increasing distance from the origin. For range expansions, this signal can be thought of as the mean allele frequency of shared alleles. At the origin, the allele frequency is expected to be lowest [35] and to increase approximately linearly with distance. However, since we do not know the allele frequency at the origin, we have to use the indirect approach by comparing pairs of populations. To be precise, if we know that shared alleles have a lower frequency at point S_i compared to point S_j , then we know that S_i is closer to the origin than S_j . If the habitat is two-dimensional, however,

505 this does not tell us the direction of the expansion. Let $\|S_i, S_j\|$ denote the Euclidean distance between
 506 two points S_i and S_j . Then,

$$\|S_i, O\| - \|S_j, O\| \approx v\psi_{i,j}, \quad (5)$$

507 where O denotes the unknown origin $\psi_{i,j}$ is the directionality index between samples S_i and S_j and v is
 508 a constant that links space to allele frequency (i.e how much does the allele frequency change per unit
 509 of space). In words, $\psi_{i,j}$ is approximately proportional to the difference of the distances $\|S_i, O\|$ and
 510 $\|S_j, O\|$ (see also Figure 5). We assume that the sampling locations of S_i and S_j are known without
 511 error, and that $\psi_{i,j}$ can be estimated from genetic data, along with its sample variance $\text{Var}(\psi_{i,j})$. We
 512 estimate the variance by doing 1,000 bootstrap replicates on the SNP. The unknowns that remain are
 513 the coordinates of the origin O and the proportionality constant v . To infer these parameters, we solve
 514 for ψ , subtract ψ from the equation and sum over all pairs of samples:

$$(\hat{O}, \hat{v}) = \underset{O, v}{\operatorname{argmax}} \sum_{i < j} \frac{1}{\text{Var}(\psi_{i,j})} \left(\frac{\|S_i, O\| - \|S_j, O\|}{v} - \psi_{i,j} \right). \quad (6)$$

515 In most biological application, space will be two-dimensional and therefore we can make this equation
 516 more explicit by writing $O = (x, y)$ and $S_i = (x_i, y_i)$. Then,

$$(\hat{x}, \hat{y}, \hat{v}) = \underset{x, y, v}{\operatorname{argmax}} \sum_{i < j} \frac{1}{\text{Var}(\psi_{i,j})} \left(\frac{1}{v} \left(\sqrt{(x_i - x)^2 + (y_i - y)^2} - \sqrt{(x_j - x)^2 + (y_j - y)^2} \right) - \psi_{i,j} \right). \quad (7)$$

517 The variance terms correspond to weighting terms; terms where ψ has a high variance are weighted down,
 518 whereas terms where we can infer ψ with high accuracy are given a larger weight. We can then find a
 519 solution to this equation using nonlinear least squares.

520 Acknowledgments

521 This research was supported in part by NIH grant R01-GM40282 to MS. We would like to thank Laurent
 522 Excoffier, Kelley Harris and Josh Schraiber for helpful discussions.

References

1. Handley LL, Estoup A, Evans DM, Thomas CE, Lombaert E, et al. (2011) Ecological genetics of invasive alien species. *BioControl* 56: 409–428.
2. Hewitt GM (1999) Post-glacial re-colonization of european biota. *Biological Journal of the Linnean Society* 68: 87–112.
3. Schmitt T (2007) Molecular biogeography of europe: Pleistocene cycles and postglacial trends. *Frontiers in Zoology* 4: 11.
4. Cavalli-Sforza LL, Menozzi P, Piazza A (1994) The history and geography of human genes. Princeton university press. URL <http://books.google.com/books?hl=en&lr=&id=FrwNcwKaUKoC&oi=fnd&pg=PP17&dq=cavalli-sforza&ots=Hl>
5. Ramachandran S, Deshpande O, Roseman CC, Rosenberg NA, Feldman MW, et al. (2005) Support from the relationship of genetic and geographic distance in human populations for a serial founder effect originating in africa. *Proceedings of the National Academy of Sciences of the United States of America* 102: 15942–15947.
6. Tishkoff SA, Reed FA, Friedlaender FR, Ehret C, Ranciaro A, et al. (2009) The genetic structure and history of africans and african americans. *Science* 324: 1035–1044.
7. Taberlet P, Fumagalli L, Wust-Saucy A, Cosson J (1998) Comparative phylogeography and post-glacial colonization routes in europe. *Molecular Ecology* 7: 453–464.
8. Wright S (1943) Isolation by distance. *Genetics* 28: 114–138.
9. Malécot G (1950) Quelques schémas probabilistes sur la variabilité des populations naturelles. In: *Annales de l'Université de Lyon A*. volume 13, p. 37–60.
10. Kimura M (1964) Diffusion models in population genetics. *Journal of Applied Probability* 1: 177–232.
11. Goldstein DB, Ruiz A, Cavalli-Sforza LL, Feldman MW (1995) An evaluation of genetic distances for use with microsatellite loci. *Genetics* 139: 463–471.

- 549 12. Nei M (1972) Genetic distance between populations. *American Naturalist* 106: 283–&.
- 550 13. Reynolds J, Weir B, Cockerham C (1983) Estimation of the Co-Ancestry coefficient - basis for a
- 551 Short-Term genetic distance. *Genetics* 105: 767–779.
- 552 14. Balakrishnan V, Sanghvi LD (1968) Distance between populations on the basis of attribute data.
- 553 *Biometrics* 24: 859–865.
- 554 15. Wright S (1949) The genetical structure of populations. *Annals of Human Genetics* 15: 323–354.
- 555 16. Weir BS, Cockerham CC (1984) Estimating F-Statistics for the analysis of population structure.
- 556 *Evolution* 38: 1358–1370.
- 557 17. Slatkin M, Voelm L (1991) F_{ST} in a hierarchical island model. *Genetics* 127: 627–629.
- 558 18. Cox JT, Durrett R (2002) The stepping stone model: New formulas expose old myths. *The Annals*
- 559 *of Applied Probability* 12: 1348–1377.
- 560 19. Pritchard JK, Stephens M, Donnelly P (2000) Inference of population structure using multilocus
- 561 genotype data. *Genetics* 155: 945–959.
- 562 20. Corander J, Waldmann P, Marttinen P, Sillanpää MJ (2004) BAPS 2: enhanced possibilities for
- 563 the analysis of genetic population structure. *Bioinformatics* 20: 2363–2369.
- 564 21. François O, Blum MGB, Jakobsson M, Rosenberg NA (2008) Demographic history of european
- 565 populations of *arabidopsis thaliana*. *PLoS Genet* 4: e1000075.
- 566 22. François O, Currat M, Ray N, Han E, Excoffier L, et al. (2010) Principal component analysis under
- 567 population genetic models of range expansion and admixture. *Molecular Biology and Evolution*
- 568 27: 1257–1268.
- 569 23. Cavalli-Sforza LL, Edwards AWF (1967) Phylogenetic analysis: Models and estimation procedures.
- 570 *Evolution* 21: 550–570.
- 571 24. Novembre J, Johnson T, Bryc K, Kutalik ZA, Boyko AR, et al. (2008) Genes mirror geography
- 572 within europe. *Nature* 456: 98–101.
- 573 25. Cavalli-Sforza LLLL, Menozzi P, Piazza A (1996) *The History and Geography of Human Genes:*
- 574 *(Abridged Paperback Edition)*. University Press.

- 575 26. Wang C, Zöllner S, Rosenberg NA (2012) A quantitative comparison of the similarity between
576 genes and geography in worldwide human populations. *PLoS Genet* 8: e1002886.
- 577 27. Hey J (2010) Isolation with migration models for more than two populations. *Molecular Biology*
578 *and Evolution* 27: 905–920.
- 579 28. Gutenkunst RN, Hernandez RD, Williamson SH, Bustamante CD (2009) Inferring the joint demo-
580 graphic history of multiple populations from multidimensional SNP frequency data. *PLoS Genet*
581 5: e1000695.
- 582 29. Menozzi P, Piazza A, Cavalli-Sforza L (1978) Synthetic maps of human gene frequencies in euro-
583 peans. *Science* 201: 786–792.
- 584 30. DeGiorgio M, Rosenberg NA (2012) Geographic sampling scheme as a determinant of the major
585 axis of genetic variation in principal components analysis. *Molecular Biology and Evolution* .
- 586 31. Austerlitz F, Jung-Muller B, Godelle B, Gouyon PH (1997) Evolution of coalescence times, genetic
587 diversity and structure during colonization. *Theoretical Population Biology* 51: 148–164.
- 588 32. Edmonds CA, Lillie AS, Cavalli-Sforza LL (2004) Mutations arising in the wave front of an expand-
589 ing population. *Proceedings of the National Academy of Sciences of the United States of America*
590 101: 975–979.
- 591 33. Hallatschek O, Hersen P, Ramanathan S, Nelson DR (2007) Genetic drift at expanding frontiers
592 promotes gene segregation. *Proceedings of the National Academy of Sciences* 104: 19926–19930.
- 593 34. DeGiorgio M, Jakobsson M, Rosenberg NA (2009) Explaining worldwide patterns of human ge-
594 netic variation using a coalescent-based serial founder model of migration outward from africa.
595 *Proceedings of the National Academy of Sciences* 106: 16057–16062.
- 596 35. Slatkin M, Excoffier L (2012) Serial founder effects during range expansion: a spatial analog of
597 genetic drift. *Genetics* 191: 171–181.
- 598 36. Durrett R (2008) Probability models for DNA sequence evolution. Springer.
- 599 37. Maruyama T (1970) Analysis of population structure. *Annals of Human Genetics* 34: 201–219.

- 600 38. Wilkins JF, Wakeley J (2002) The coalescent in a continuous, finite, linear population. *Genetics*
601 161: 873–888.
- 602 39. Busing FMTA, Meijer E, Leeden RVD (1999) Delete-m jackknife for unequal m. *Statistics and*
603 *Computing* 9: 3–8.
- 604 40. Reich D, Thangaraj K, Patterson N, Price AL, Singh L (2009) Reconstructing indian population
605 history. *Nature* 461: 489–494.
- 606 41. Gustafsson F, Gunnarsson F (2003) Positioning using time-difference of arrival
607 measurements. In: *Acoustics, Speech, and Signal Processing, 2003. Proceed-*
608 *ings(ICASSP'03). 2003 IEEE International Conference on.* volume 6, p. VI–553. URL
609 http://ieeexplore.ieee.org/xpls/abs_all.jsp?arnumber=1201741.
- 610 42. Wegmann D, Currat M, Excoffier L (2006) Molecular diversity after a range expansion in hetero-
611 geneous environments. *Genetics* 174: 2009–2020.
- 612 43. Aho AV, Garey MR, Ullman JD (1972) The transitive reduction of a directed graph. *SIAM Journal*
613 *on Computing* 1: 131–137.
- 614 44. Korte BBH, Vygen J (2008) *Combinatorial Optimization: Theory and Algorithms*. Springer Lon-
615 don, Limited.
- 616 45. Fumagalli M, Sironi M, Pozzoli U, Ferrer-Admettla A, Pattini L, et al. (2011) Signatures of en-
617 vironmental genetic adaptation pinpoint pathogens as the main selective pressure through human
618 evolution. *PLoS Genetics* 7: e1002355.
- 619 46. Cann HM, De Toma C, Cazes L, Legrand M, Morel V, et al. (2002) A human genome diversity
620 cell line panel. *Science* 296: 261–262.
- 621 47. TIHC (2010) Integrating common and rare genetic variation in diverse human populations. *Nature*
622 467: 52.
- 623 48. Henn BM, Gignoux CR, Jobin M, Granka JM, Macpherson JM, et al. (2011) Hunter-Gatherer ge-
624 nomic diversity suggests a southern african origin for modern humans. *Proceedings of the National*
625 *Academy of Sciences* .

49. Beaumont MA, Zhang W, Balding DJ (2002) Approximate bayesian computation in population genetics. *Genetics* 162: 2025–2035.
50. Wegmann D, Leuenberger C, Neuenschwander S, Excoffier L (2010) ABCtoolbox: a versatile toolkit for approximate bayesian computations. *BMC Bioinformatics* 11: 116.
51. Rosenberg NA, Mahajan S, Ramachandran S, Zhao C, Pritchard JK, et al. (2005) Clines, clusters, and the effect of study design on the inference of human population structure. *PLoS Genet* 1: e70.
52. Guillot G, Leblois R, Coulon A, Frantz AC (2009) Statistical methods in spatial genetics. *Molecular Ecology* 18: 4734–4756.
53. Rasmussen M, Guo X, Wang Y, Lohmueller KE, Rasmussen S, et al. (2011) An aboriginal australian genome reveals separate human dispersals into asia. *Science* 334: 94–98.
54. Wakeley J (2009) *Coalescent theory: an introduction*. Roberts & Co. Publishers.

Figure Legends

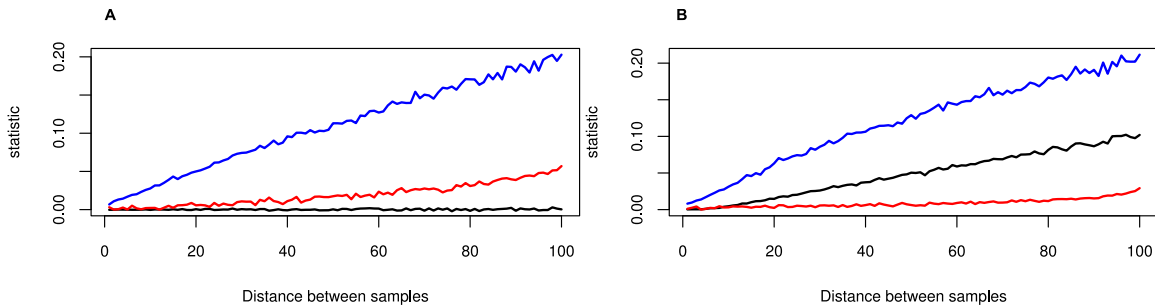


Figure 1. Behavior of H (red), ψ (black) and F_{ST} (blue) in one-dimensional (A) isolation-by-distance and (B) population-expansion models. Simulations were performed on a 200-stepping stone model with scaled migration rate $M=100$ between adjacent demes, and expansion events every 0.001 coalescence units. F_{ST} increases linearly with distance in both models and ψ is zero in the isolation-by-distance model, but increases approximately linearly in the expansion model. Heterozygosity increases from the center of the population (left) to the border of the habitat (right).

Tables

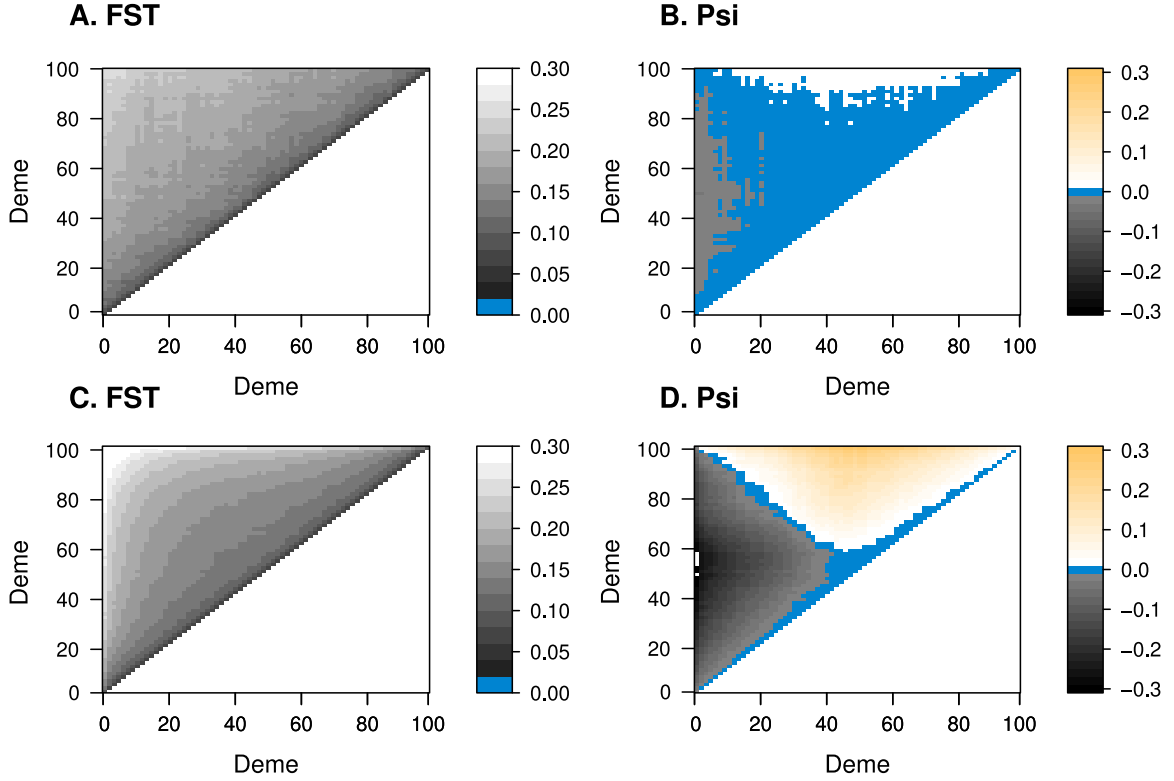


Figure 2. Behavior of F_{ST} and ψ in isolation-by-distance and population expansion model.

Each panel gives the value of the pairwise statistics F_{ST} (Panels A and C) and ψ (Panels B and D) under an isolation-by-distance model (Panels A and B) and an expansion model (Panels C and D) starting in the central deme (50,50). Simulations were performed on a 101 x 101 deme stepping stone model, and a diagonal transect from demes at coordinates (0,0) to (100,100) was sampled, and all pairwise statistics were calculated. Blue regions correspond to regions where F_{ST} and ψ are very low (below 1%). The orange and grey regions denote areas with positive and negative ψ , respectively. Whereas F_{ST} behaves qualitatively similar under both models, the behavior of ψ is very different. Under isolation-by-distance, ψ is very close to zero, with some deviations due to boundary effects. Under an expansion, however, we see a clear signal of an expansion for all demes, except demes that are very close to each other, or demes that have the same distance to the origin, but in different directions.

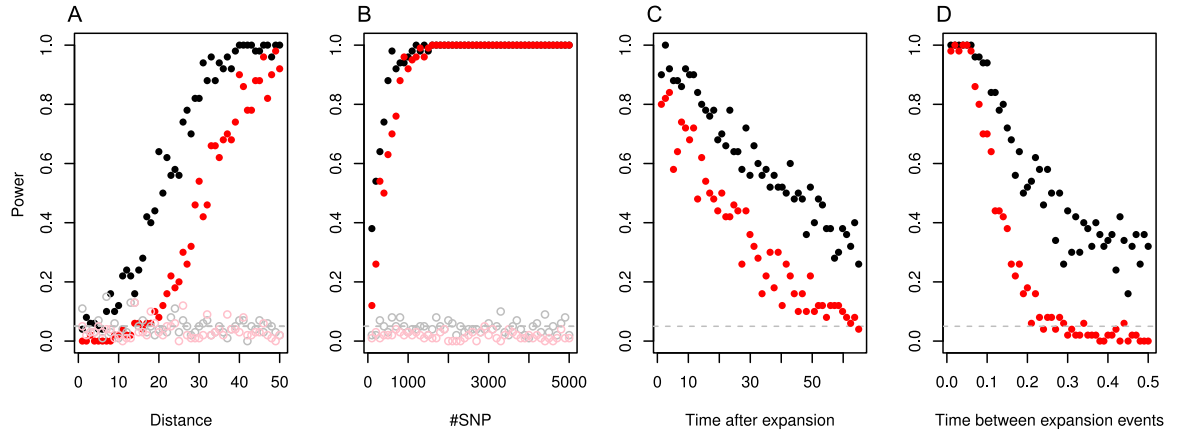


Figure 3. True/false positive rates of detecting range expansion Each panel give the proportion of replicates in which the null model was rejected at the 5% significance level. Filled dots denote simulations under an expansion model, and open dots correspond to an isolation-by-distance model. Black dots corresponds to using the directionality index, and the red dots were generated using the difference in heterozygosity as a statistic. The grey dashed line at 0.05 gives the expected proportion of false positives under the null hypothesis. Baseline parameters for the simulations were of 2 chromosomes (one diploid individual) at each location sampled, with locations a distance of 50 each other. Each sample consisted of 1,000 independent SNPs shared between the two populations. Significance was assessed using a binomial test.

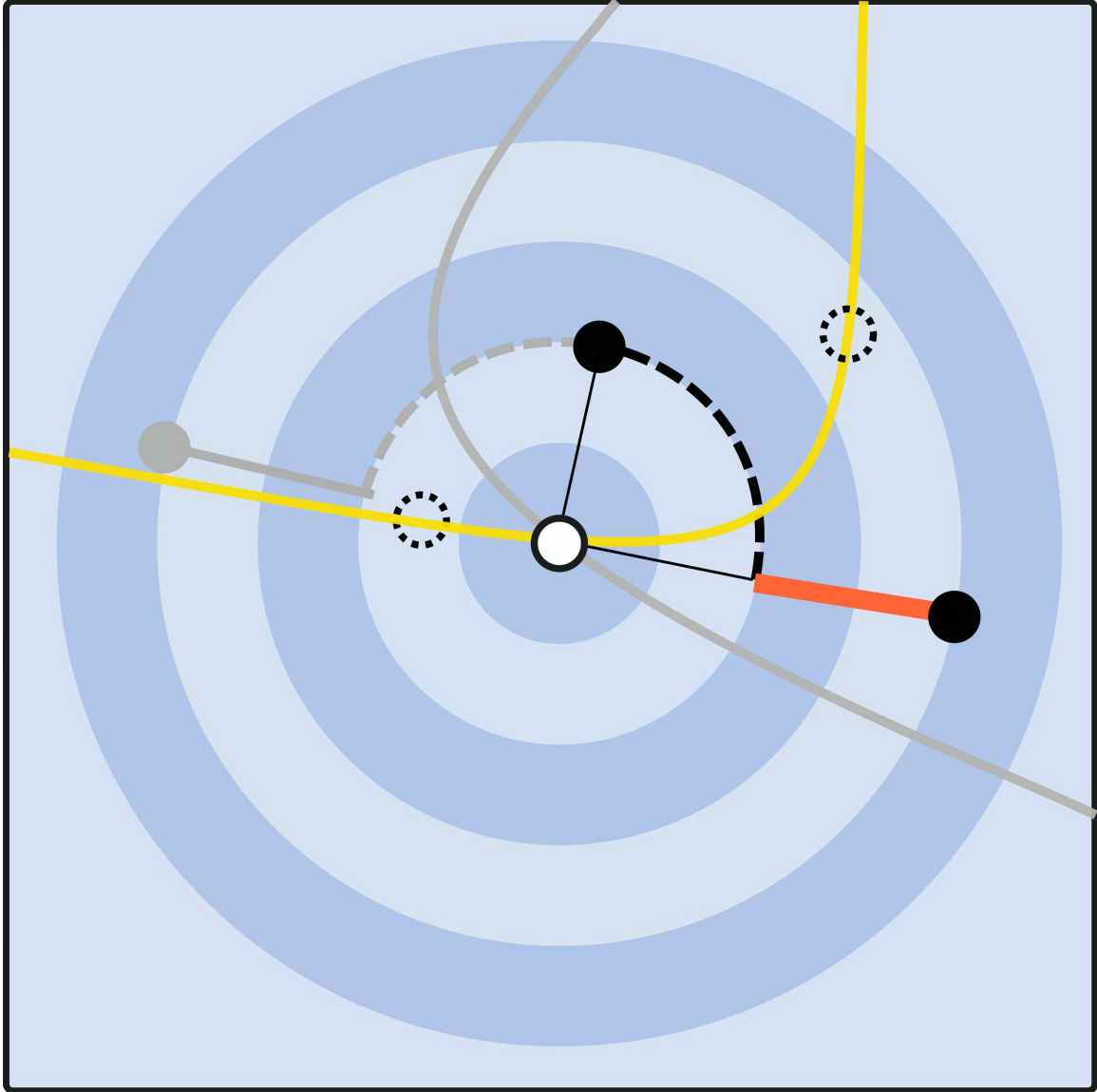


Figure 4. Illustration of the method used to infer the origin of a range expansion. The black and grey points correspond to genetic samples taken, the white point corresponds to the (unknown) origin of the expansion. Using the directionality index ψ , we can infer the difference in distance from the samples to the origin (orange line). The set of all points that has the same difference in distance to the origin corresponds to the arm of a hyperbola (yellow), with some candidate points outlined with the dashed point. Using a second pair of points (the grey and top black point), we can identify a second hyperbola, and find an unique location of the origin. In practice, we use more than three sampling locations. Sampling noise will cause the hyperbolas to not intersect in a single point. We use a least-squares criterion to estimate the location of the origin.

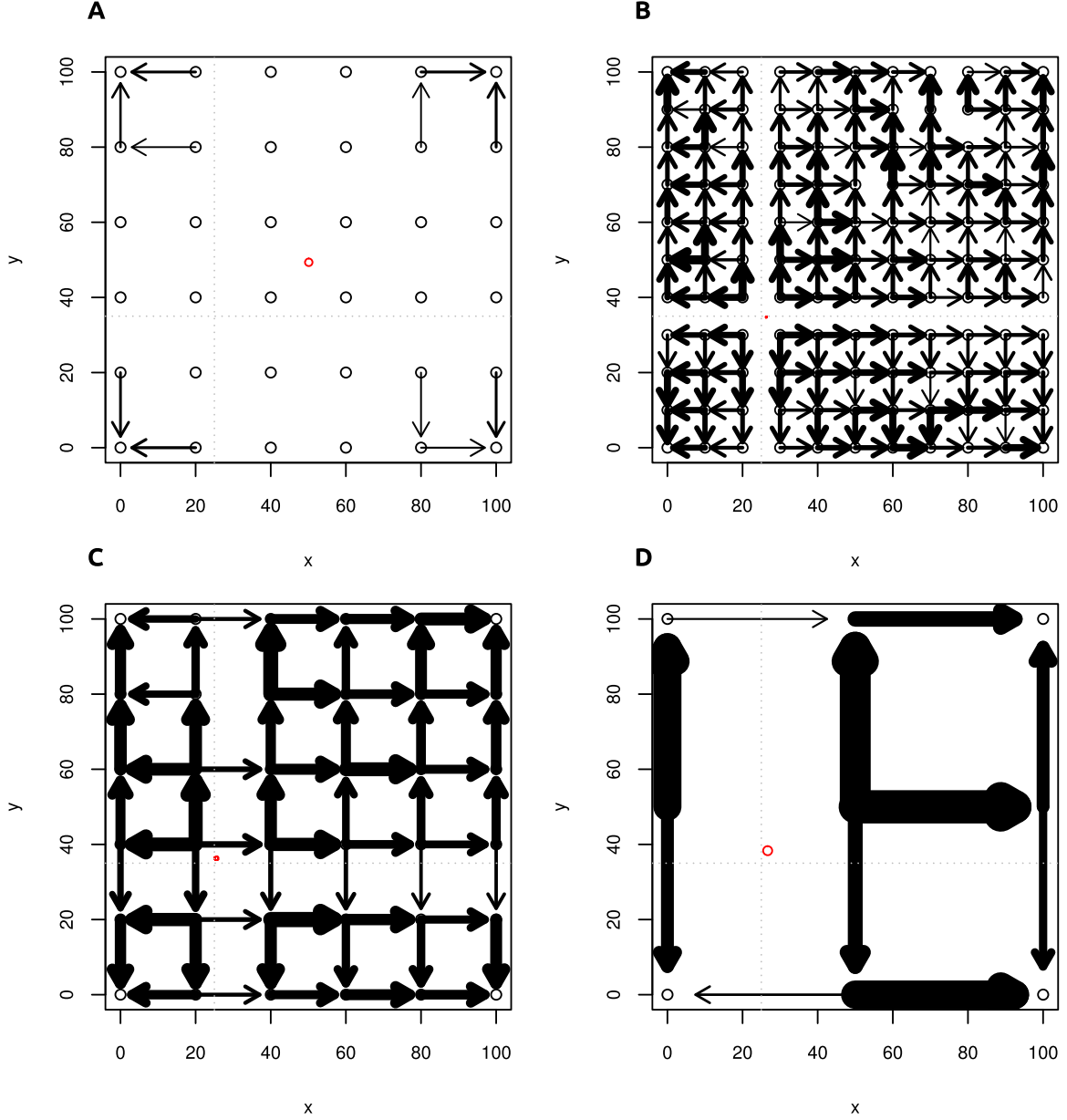


Figure 5. Detecting the origin of a range expansion. Each panel corresponds to a 101 x 101 grid of populations that were simulated. The expansion began at point (25,35) (indicated by gray dotted lines). Black bordered circles indicate sampling locations, black arrows correspond to $\psi > 1\%$ between adjacent samples, with the direction of the arrow indicating the sign of ψ . Thicker arrows correspond to larger ψ . The red ellipse corresponds to the 95% confidence interval of the estimated location of the origin. Panel a: no expansion (isolation-by-distance model). Edge effects cause the estimated origin to be close to the center of the grid of populations. Panels b-d: Expansion with parameters $M = 1$, $t = 0.1$ and samples taken every 10th, 20th and 50th deme. While the confidence region is larger for smaller numbers of samples, we get a very accurate result even when we have only 9 samples.

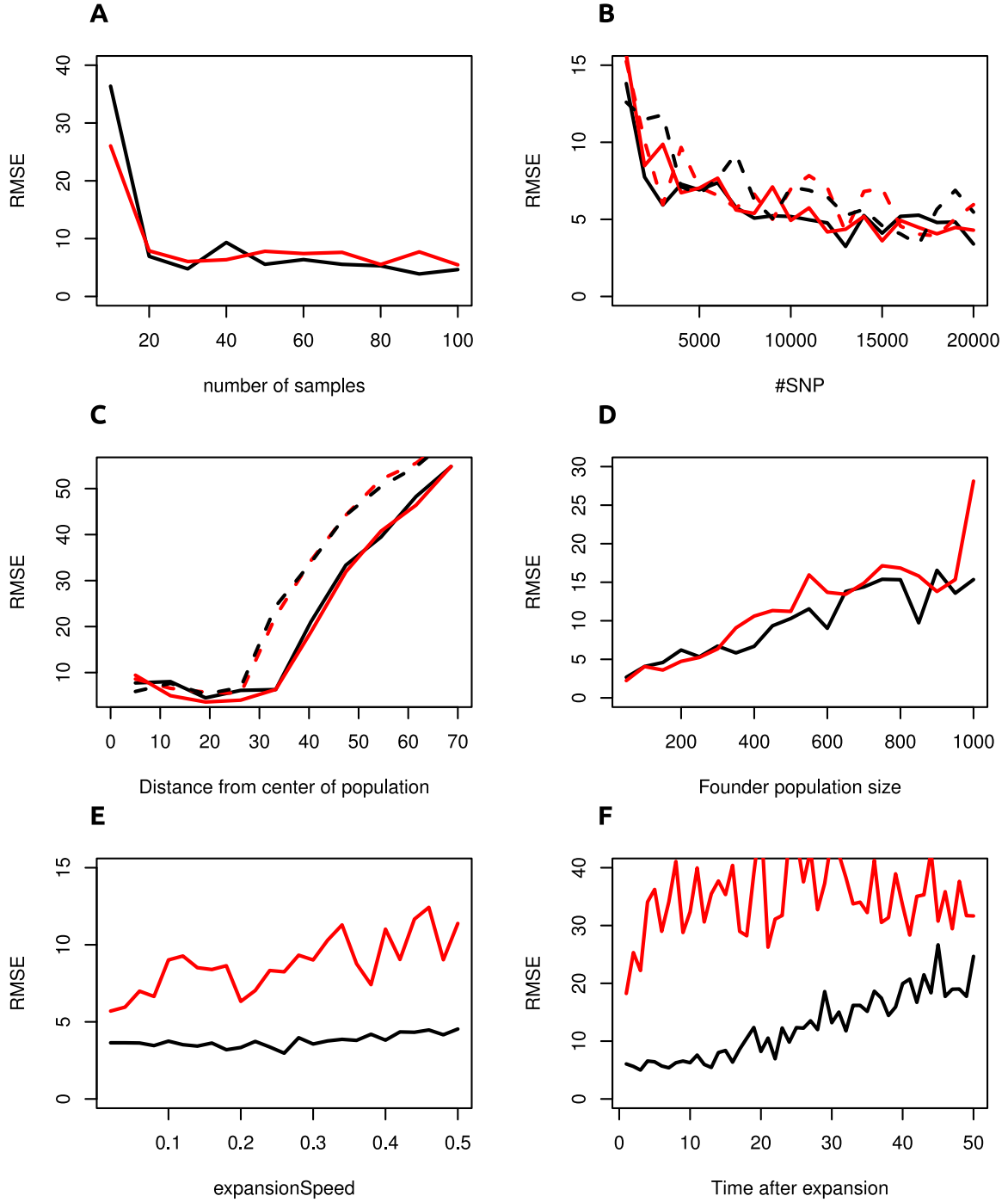


Figure 6. Performance of TDOA method. We present the root mean squared errors of our TDOA method (black) compare it with the method of Ramachandran et al. 2005 (red). Samples taken on a grid were represented by full lines, whereas dashed lines denote samples that were taken from random coordinates in the simulated region. Our method is superior when the expansion occurred slowly or when it finished some time in the past; but the method perform very similar for recent, fast expansions.

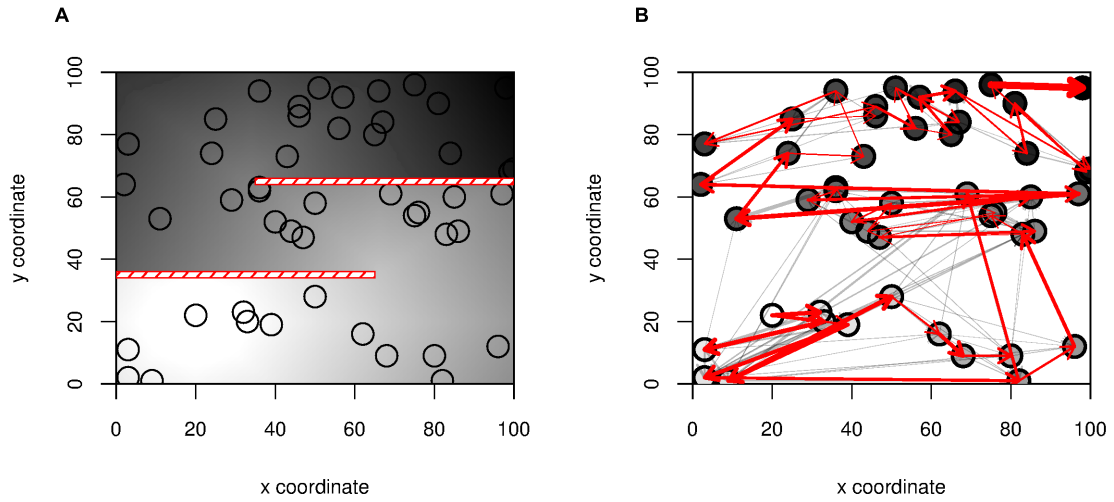


Figure 7. Identifying complex patterns of migration. We simulated data on a S-shaped habitat with two impermeable barriers (Panel A) The darkness of the shading is proportional to the arrival time of the expansion, which began in deme (20,20). Black circles correspond to locations sampled. In Panel B we show the inferred pairwise directionality, with all edges remaining after thinning the graph shown in grey, and a maximum spanning tree in red. We also show the inferred ordering of the samples as a color gradient of the samples from light (closest to origin) to dark. The barriers can be identified from panel B by the absence of any indication of gene flow across the barriers and by examining the ordering of the samples.

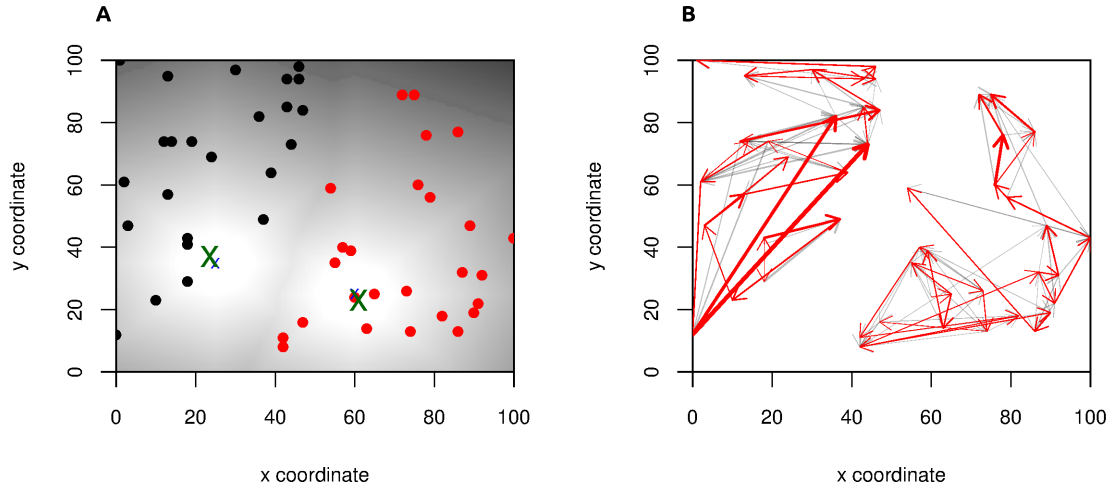


Figure 8. Detecting multiple origins. Panel a: We simulated two expansions that originated at the same time from origins indicated by the blue crosses. The color gradient in the background corresponds to the time of colonization time of each deme. We address the problem of inferring the origin of multiple expansions using a two-step procedure. First, we cluster the samples into discrete clusters (red and black, respectively) and then estimate the expansion signal and origins independently for the clusters, resulting in high accuracy for both origins (green X). The right panel shows the inferred migration patterns after a transitive reduction (grey/red arrows) and a maximum spanning tree (red arrows).

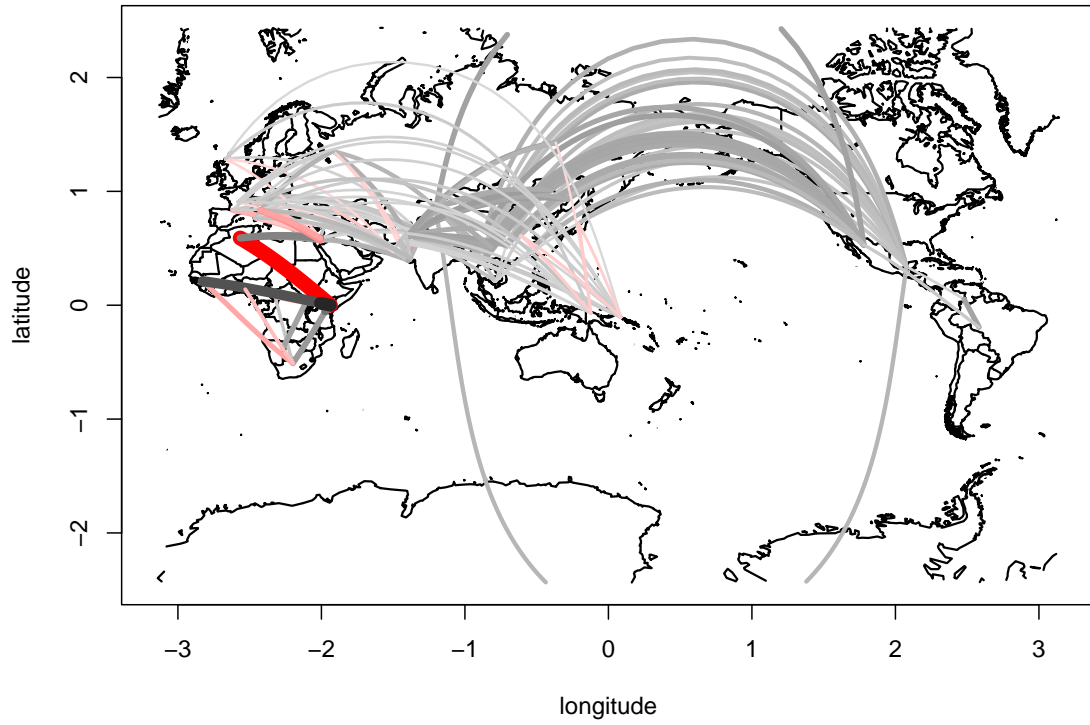


Figure 9. Inference of human migration routes. The figure shows a visual representation of the pairwise directionality indices between human populations in HGDP and HapMap. Each line corresponds to the pairwise ψ statistic, with thicker and brighter lines corresponding to higher values. Grey and red lines denote eastward and westward migration, respectively. Lines with an absolute Z-score below 5 were omitted.

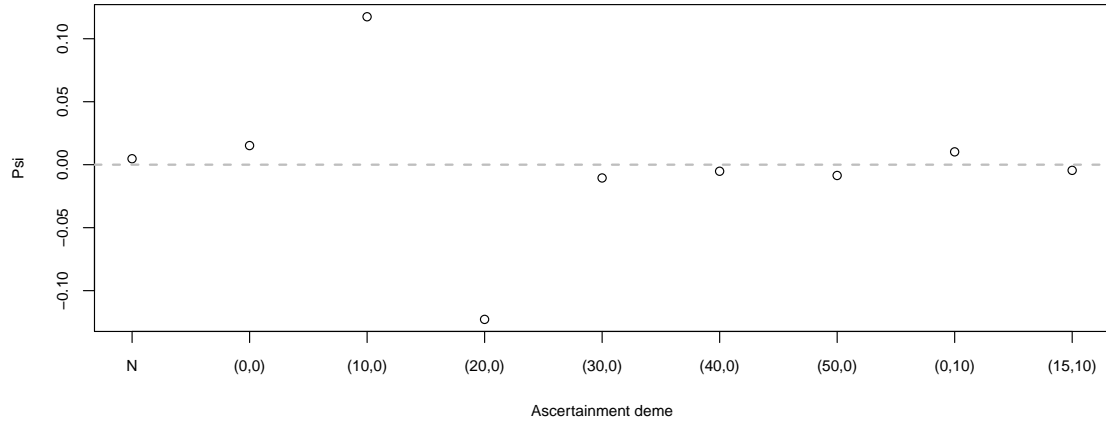


Figure 10. Effect of ascertainment bias on ψ . We show the effect of strong ascertainment bias in different demes given on the x-axis on ψ calculated between samples taken from coordinates (0,10) and (0,20). N = no ascertainment. Ascertainment has very little effect if it is performed in a deme that is not used in the comparison.